



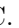












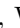
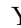








# Observation of the decays $B^+ \rightarrow \Sigma_c(2455)^{++}\bar{\Xi}_c'^-$ and $B^0 \rightarrow \Sigma_c(2455)^0\bar{\Xi}_c'^0$

M. Abumusabh , A. Aggarwal , H. Ahmed , J. K. Ahn , Y. Ahn , M. Akdag , N. Akopov , S. Alghamdi ,  
M. Alhakami , N. Althubiti , K. Amos , M. Angelsmark , N. Anh Ky , C. Antonioli , K. Arai ,  
H. Atmacan , T. Aushev , V. Aushev , R. Ayad , V. Babu , H. Bae , N. K. Baghel , S. Bahinipati ,  
P. Bambade , Sw. Banerjee , M. Barrett , M. Bartl , J. Baudot , A. Beaubien , F. Becherer , J. Becker ,  
G. F. Benfratello , J. V. Bennett , F. U. Bernlochner , V. Bertacchi , M. Bertemes , E. Bertholet ,  
M. Bessner , S. Bettarini , V. Bhardwaj , B. Bhuyan , F. Bianchi , T. Bilka , D. Biswas , A. Bobrov ,  
D. Bodrov , G. Bonvicini , J. Borah , A. Boschetti , A. Bozek , M. Bračko , P. Branchini ,  
R. A. Briere , T. E. Browder , A. Budano , S. Bussino , Q. Campagna , M. Campajola , M. Carminati ,  
G. Casarosa , C. Cecchi , P. Cheema , L. Chen , B. G. Cheon , C. Cheshta , H. Chetri , K. Chilikin ,  
K. Chirapatpimol , H.-E. Cho , K. Cho , S.-J. Cho , S.-K. Choi , S. Choudhury , S. Chutia , J. Cochran ,  
J. A. Colorado-Caicedo , I. Consigny , L. Corona , S. Cuccuini , J. X. Cui , E. De La Cruz-Burelo ,  
S. A. De La Motte , G. De Nardo , G. De Pietro , R. de Sangro , M. Destefanis , S. Dey , R. Dhayal ,  
A. Di Canto , J. Dingfelder , Z. Doležal , X. Dong , M. Dorigo , G. Dujany , P. Ecker , D. Epifanov ,  
J. Eppelt , R. Farkas , P. Feichtinger , T. Ferber , T. Fillinger , C. Finck , G. Finocchiaro , F. Forti ,  
B. G. Fulsom , P. Gagneja , R. Garg , A. Garmash , G. Gaudino , V. Gaur , V. Gautam , A. Gaz ,  
A. Gellrich , G. Ghevondyan , D. Ghosh , H. Ghumaryan , R. Giordano , A. Giri , P. Gironella Gironell ,  
B. Gobbo , R. Godang , O. Gogota , W. Gradl , E. Graziani , D. Greenwald , K. Gudkova , Y. Han ,  
K. Hayasaka , H. Hayashii , S. Hazra , C. Hearty , M. T. Hedges , A. Heidelberg , G. Heine ,  
I. Heredia de la Cruz , T. Higuchi , M. Hoek , M. Hohmann , R. Hoppe , P. Horak , X. T. Hou ,  
C.-L. Hsu , T. Humair , T. Iijima , K. Inami , N. Ipsita , A. Ishikawa , R. Itoh , M. Iwasaki , P. Jackson ,  
D. Jacobi , W. W. Jacobs , E.-J. Jang , Q. P. Ji , S. Jia , Y. Jin , A. Johnson , K. K. Joo , H. Kakuno ,  
K. H. Kang , G. Karyan , F. Keil , C. Ketter , C. Kiesling , C. Kim , D. Y. Kim , H. Kim , J.-Y. Kim ,  
K.-H. Kim , H. Kindo , K. Kinoshita , P. Kodyš , S. Kohani , A. Korobov , S. Korpar , E. Kovalenko ,  
R. Kowalewski , P. Križan , P. Krokovny , T. Kuhr , Y. Kulii , R. Kumar , K. Kumara , T. Kunigo ,  
S. Kurokawa , A. Kuzmin , Y.-J. Kwon , S. Lacaprra , Y.-T. Lai , T. Lam , J. S. Lange , T. S. Lau ,  
R. Leboucher , M. J. Lee , P. Leo , P. M. Lewis , C. Li , L. K. Li , Q. M. Li , S. X. Li , W. Z. Li , Y. Li ,  
Y. B. Li , Y. P. Liao , J. Libby , J. Lin , S. Lin , Z. Liptak , V. Lisovskiy , C. Liu , M. H. Liu ,  
Q. Y. Liu , Z. Q. Liu , D. Liventsev , S. Longo , A. Lozar , T. Lueck , C. Lyu , J. L. Ma , Y. Ma ,  
M. Maggiora , S. P. Maharana , R. Maiti , G. Mancinelli , R. Manfredi , E. Manoni , M. Mantovano ,  
D. Marcantonio , S. Marcello , M. Marfoli , C. Marinas , C. Martellini , A. Martens , T. Martinov ,  
L. Massaccesi , M. Masuda , T. Matsuda , D. Matvienko , S. K. Maurya , M. Maushart , J. A. McKenna ,  
Z. Mediankin Gruberová , R. Mehta , F. Meier , D. Meleshko , M. Merola , C. Miller , M. Mirra ,  
K. Miyabayashi , H. Miyake , R. Mizuk , S. Moneta , A. L. Moreira de Carvalho , H.-G. Moser , N. Mudgal ,  
Th. Muller , H. Murakami , R. Mussa , M. Nakao , Y. Nakazawa , Z. Natkaniec , A. Natochii , M. Nayak ,  
M. Neu , M. Niiyama , S. Nishida , R. Nomaru , S. Ogawa , R. Okubo , H. Ono , G. Pakhlova ,  
S. Pardi , J. Park , K. Park , S.-H. Park , A. Passeri , S. Patra , T. K. Pedlar , L. E. Piilonen ,  
P. L. M. Podesta-Lerma , T. Podobnik , L. Polat , A. Prakash , R. pramanik , V. Prasad , S. Prell ,  
E. Prencipe , M. T. Prim , H. Purwar , P. Rados , S. Raiz , K. Ravindran , J. U. Rehman , M. Reif ,  
S. Reiter , M. Remnev , L. Reuter , D. Ricalde Herrmann , I. Ripp-Baudot , G. Rizzo , S. H. Robertson ,  
J. M. Roney , A. Rostomyan , N. Rout , G. Russo , S. Saha , G. Sanchez , D. A. Sanders , S. Sandilya ,  
L. Santelj , C. Santos , V. Savinov , B. Scavino , J. Schmitz , S. Schneider , G. Schnell , K. Schoenning ,  
C. Schwanda , Y. Seino , K. Senyo , J. Serrano , C. Sfienti , W. Shan , C. P. Shen , X. D. Shi ,  
T. Shillington , T. Shimasaki , J.-G. Shiu , D. Shtol , A. Sibidanov , F. Simon , J. B. Singh , J. Skorupa ,  
A. Soffer , A. Sokolov , E. Solovieva , S. Spataro , K. Špenko , B. Spruck , M. Starič , P. Stavroulakis ,  
S. Stefkova , R. Stroili , M. Sumihama , M. Takahashi , M. Takizawa , U. Tamponi , S. S. Tang ,  
K. Tanida , F. Testa , A. Thaller , D. V. Thanh , T. Tien Manh , O. Tittel , R. Tiwary , E. Torassa ,  
F. F. Trantou , I. Tsaklidis , M. Uchida , I. Ueda , T. Uglov

S. Watanuki , C. Wessel , X. P. Xu , B. D. Yabsley , S. Yamada , W. Yan , W. P. Yan , J. Yelton , K. Yi , J. H. Yin , K. Yoshihara , C. Z. Yuan , J. Yuan , L. Yuan , Y. Yusa , L. Zani , F. Zeng , M. Zeyrek , B. Zhang , X. Zhao , V. Zhilich , J. S. Zhou , Q. D. Zhou , L. Zhu , and R. Žlebčik 

(The Belle and Belle II Collaborations)

We report the first observation of the decays  $B^+ \rightarrow \Sigma_c(2455)^{++}\bar{\Xi}'_c{}^-$  and  $B^0 \rightarrow \Sigma_c(2455)^0\bar{\Xi}'_c{}^0$ , with significances of  $6.4\sigma$  and  $5.3\sigma$ , respectively, including systematic uncertainties. This analysis is based on data samples containing  $771.6 \times 10^6$   $\Upsilon(4S)$  decays collected with the Belle detector at the KEKB collider and  $520.6 \times 10^6$   $\Upsilon(4S)$  decays collected with the Belle II detector at the SuperKEKB collider. The branching fractions are measured to be  $\mathcal{B}(B^+ \rightarrow \Sigma_c(2455)^{++}\bar{\Xi}'_c{}^-) = (1.68 \pm 0.31 \pm 0.12_{-0.54}^{+1.49}) \times 10^{-3}$  and  $\mathcal{B}(B^0 \rightarrow \Sigma_c(2455)^0\bar{\Xi}'_c{}^0) = (1.28 \pm 0.32 \pm 0.10_{-0.21}^{+0.30}) \times 10^{-3}$ , where the first and second uncertainties are statistical and systematic, respectively, and the third arises from the uncertainties in the absolute branching fractions of  $\bar{\Xi}'_c{}^-$  and  $\bar{\Xi}'_c{}^0$  decays. This result represents the first observation of  $B$ -meson decays into a pair of charmed baryon-antibaryon states belonging to the same  $SU(3)$  flavor sextet.

$B$ -meson decays provide a unique laboratory to explore the interplay between weak and strong interactions in the nonperturbative regime of quantum chromodynamics. Two-body baryonic  $B$  decays proceed at tree level through  $W$ -exchange,  $W$ -annihilation, and internal  $W$ -emission topologies [1, 2]. The factorizable  $W$ -exchange and  $W$ -annihilation contributions are expected to be helicity suppressed [3]. However, in contrast to mesonic  $B$  decays, the internal  $W$ -emission contribution is not necessarily color suppressed, and can therefore play a dominant role in baryonic two-body decays [3–5]. The large mass of the  $B$  meson allows for decays into charmed baryon-antibaryon pairs. Over the past two decades, several such modes have been observed [6–9]. The branching fractions of  $B$ -meson decays into charmed baryon-antibaryon pairs are significantly larger than those of two-body decays containing one charmed baryon and one charmless baryon, and both exceed those of fully charmless baryonic decays, reaching values as large as  $\mathcal{O}(10^{-3})$  [10].

Recently, the decays  $B^+ \rightarrow \Sigma_c(2455)^{++}\bar{\Xi}'_c{}^-$  and  $B^0 \rightarrow \Sigma_c(2455)^0\bar{\Xi}'_c{}^0$  were observed for the first time, by the Belle and Belle II experiments [11], with branching fractions measured to be of the order of  $10^{-4}$ . These modes proceed through internal  $W$ -emission topology. The  $\bar{\Xi}'_c{}^-$  and  $\bar{\Xi}'_c{}^0$  baryons share the same valence-quark content but in a heavy quark and light diquark model differ in the spin configuration of the light diquark. Consequently, the decays  $B^+ \rightarrow \Sigma_c(2455)^{++}\bar{\Xi}'_c{}^-$  and  $B^0 \rightarrow \Sigma_c(2455)^0\bar{\Xi}'_c{}^0$  are expected to proceed through the same internal  $W$ -emission topology, as illustrated in Fig. 1. A comparison between the branching fractions of  $B \rightarrow \Sigma_c(2455)\bar{\Xi}'_c$  and  $B \rightarrow \Sigma_c(2455)\bar{\Xi}_c$  could provide insight into the underlying dynamics of  $B$  decays to charmed baryon-antibaryon pairs belonging to different  $SU(3)$  flavor multiplets. To date, there have been no observations of  $B$  decays into charmed baryon-antibaryon pairs in which both daughters belong to a flavor sextet.

In this paper, we report the first measurement of the decays  $B^+ \rightarrow \Sigma_c(2455)^{++}\bar{\Xi}'_c{}^-$  and  $B^0 \rightarrow \Sigma_c(2455)^0\bar{\Xi}'_c{}^0$ . Most of the selection criteria follow those in Ref. [11].

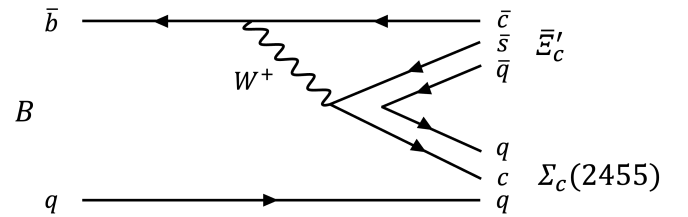


FIG. 1: Diagram illustrating the internal  $W$ -emission topology for the decays  $B^+ \rightarrow \Sigma_c(2455)^{++}\bar{\Xi}'_c{}^-$  and  $B^0 \rightarrow \Sigma_c(2455)^0\bar{\Xi}'_c{}^0$ , corresponding to  $q = u$  and  $q = d$ , respectively.

In addition there are further requirements related to the additional photon from the  $\bar{\Xi}'_c$  decay. The  $\Sigma_c(2455)^{++}$  baryons are reconstructed via their decays into  $\Lambda_c^+\pi^\pm$ , with the  $\Lambda_c^+$  reconstructed using the  $\Lambda_c^+ \rightarrow pK^-\pi^+$  and  $\Lambda_c^+ \rightarrow pK_S^0$  modes. The  $\bar{\Xi}'_c{}^{-,0}$  baryons are reconstructed via their decays into  $\gamma\bar{\Xi}_c{}^{-,0}$ , with the  $\bar{\Xi}_c{}^-$  reconstructed using the  $\bar{\Xi}_c^- \rightarrow \bar{\Xi}^+\pi^-\pi^-$  and  $\bar{\Xi}_c^- \rightarrow \bar{p}K^+\pi^-$  modes and the  $\bar{\Xi}_c^0$  reconstructed using the  $\bar{\Xi}_c^0 \rightarrow \bar{\Xi}^+\pi^-$  and  $\bar{\Xi}_c^0 \rightarrow \bar{\Lambda}K^+\pi^-$  modes. Charge-conjugate channels are implicitly included throughout this paper. This study is based on data samples containing  $(771.6 \pm 10.6) \times 10^6$  and  $(520.6 \pm 7.6) \times 10^6$   $\Upsilon(4S)$  events collected with the Belle [12] and Belle II [13] detectors, respectively, at the  $e^+e^-$  center-of-mass energy ( $\sqrt{s}$ ) of 10.58 GeV, corresponding to integrated luminosities of  $711 \text{ fb}^{-1}$  [14] and  $492 \text{ fb}^{-1}$  [15]. The analysis strategy is to fully reconstruct the signal decay chains and extract the signal yields from simultaneous fits to the distributions of the difference between the reconstructed  $B$ -meson energy and the beam energy at the  $\Upsilon(4S)$  rest frame, both in the  $\bar{\Xi}'_c$  signal and sideband regions.

The Belle detector was a cylindrical large-solid-angle magnetic spectrometer located at the interaction point (IP) of the KEKB asymmetric-energy  $e^+e^-$  collider [16]. The detector consisted of a silicon vertex detector (SVD), a central drift chamber (CDC), an array of aerogel threshold Cherenkov counters (ACC), a barrel-like arrangement of time-of-flight (TOF) scintillation counters, and an electromagnetic

calorimeter (ECL) composed of CsI(Tl) crystals located inside a superconducting solenoid coil that provided a 1.5 T axial magnetic field. An iron flux-return located outside the coil was instrumented to detect  $K_L^0$ -mesons and to identify muons. A detailed description of the Belle detector can be found in Ref. [12].

The Belle II detector, located at the SuperKEKB asymmetric-energy  $e^+e^-$  collider [17], is an upgraded version of the Belle detector. Belle II includes a SVD consisting of pixel sensors and double-sided strip detectors, and a CDC. The CDC is surrounded by two types of Cherenkov light detector systems: time-of-propagation (TOP) detector for the barrel region and an aerogel ring-imaging Cherenkov (ARICH) detector for the forward end-cap region. The Belle ECL is reused in Belle II along with the solenoid and the iron flux-return yoke. However, the ECL readout system has been upgraded. The solenoid flux return is instrumented with resistive-plate chambers and plastic scintillator modules to detect muons and  $K_L^0$  mesons. A detailed description of the Belle II detector can be found in Ref. [13].

Simulated signal events are used to optimize the selection criteria, calculate the reconstruction efficiencies, and determine the fit models. The EVTGEN [18] and PYTHIA [19, 20] software packages are used to generate  $e^+e^- \rightarrow \Upsilon(4S) \rightarrow B\bar{B}$  events with final-state radiation simulated by the PHOTOS software package [21]. In the simulation, one  $B$  meson is not constrained to decay into a specific final state, while the other decays into a signal mode. The simulation includes beam-induced background data overlay [22]. Inclusive simulated samples of  $e^+e^- \rightarrow q\bar{q}$  ( $q = u, d, s, c$ ) and  $\Upsilon(4S) \rightarrow B\bar{B}$  are used to optimize the selection criteria and identify the background sources [23], corresponding to six times the integrated luminosity of the Belle data and four times that of the Belle II data. The KKMC [24] and PYTHIA [19, 20] software packages are used to simulate the  $e^+e^- \rightarrow q\bar{q}$  processes. The detector responses are modeled by the software packages GEANT3 [25] for Belle and GEANT4 [26] for Belle II.

We analyze both Belle and Belle II data using the Belle II analysis software framework [27]. For the Belle data, the event reconstruction up to the particle level is performed with the Belle software, and the reconstructed data are then converted into a Belle II compatible format [28]. This allows the Belle and Belle II samples to be analyzed within a unified framework. To avoid experimental bias, the signal region was not examined until the analysis procedure was finalized. All selection criteria are determined by iteratively optimizing the Punzi figure-of-merit for a target significance of five standard deviations in simulation [29]. We apply identical event-selection criteria in the Belle and Belle II analyses, unless otherwise stated.

We select tracks, except for those from the decays of  $K_S^0$ ,  $\bar{\Lambda}$ , and  $\bar{\Xi}^+$ , by requiring the impact parameters relative to the  $e^+e^-$  IP to be less than 2.0 cm

perpendicular to the  $z$ -axis and less than 4.0 cm parallel to it. The  $z$ -axis is defined as the central solenoid axis with the positive direction in the  $e^-$  beam direction, common to both Belle and Belle II. The identification of charged tracks uses the likelihood ratio  $\mathcal{R}(h|h') = \mathcal{L}(h)/[\mathcal{L}(h) + \mathcal{L}(h')]$ , where  $\mathcal{L}(h^{(i)})$  is the likelihood of the charged track being a hadron  $h^{(i)} = p, K, \text{ or } \pi$ . This likelihood ratio is determined with a particle identification (PID) algorithm that combines information from different detector subsystems, including the specific ionization in the CDC, time-of-flight measurement in the TOF (TOP), and the response of the ACC (ARICH) in Belle (Belle II) [30, 31]. Correction factors derived from control samples in data are applied to account for differences between data and simulation in tracking and PID efficiencies. Tracks with  $\mathcal{R}(p|K) > 0.6$  and  $\mathcal{R}(p|\pi) > 0.6$  are identified as proton candidates; charged kaon (pion) candidates must satisfy  $\mathcal{R}(K|\pi) > 0.6$  ( $< 0.4$ ). The efficiencies of these requirements range from 80% to 95%, with corresponding misidentification rates between 3% and 9%. The pion candidates used to reconstruct the  $K_S^0$ ,  $\bar{\Lambda}$ , and  $\bar{\Xi}^+$  candidates are exempt from PID requirements as their kinematics provide sufficient discrimination.

The  $K_S^0$  candidates are reconstructed from pairs of oppositely charged tracks treated as pions. An artificial neural network [32] and a boosted decision tree (BDT) classifier [33] are used in Belle and Belle II, respectively, to select the  $K_S^0$  candidates. The  $\bar{\Lambda}$  candidates are reconstructed from the decay  $\bar{\Lambda} \rightarrow \bar{p}\pi^+$  and selected using momentum-dependent requirements on variables describing the displaced decay topology in Belle [34] and using a BDT classifier in Belle II. These discriminators primarily rely on the kinematic properties of the  $K_S^0$  or  $\bar{\Lambda}$  and their decay products. The invariant masses of the  $K_S^0$  and  $\bar{\Lambda}$  candidates are required to be within  $\pm 9.0 \text{ MeV}/c^2$  and  $\pm 5.5 \text{ MeV}/c^2$  of their known masses [10], respectively, corresponding to approximately 2.5 times the mass resolution ( $\sigma$ ). The selected  $\bar{\Lambda}$  candidate is then combined with a  $\pi^+$  candidate to form a  $\bar{\Xi}^+$  candidate. The invariant mass of  $\bar{\Xi}^+$  candidates is required to be within  $\pm 6.5 \text{ MeV}/c^2$  of its known mass [10] (approximately  $2.5\sigma$ ). A vertex fit is performed for each  $K_S^0$ ,  $\bar{\Lambda}$ , and  $\bar{\Xi}^+$  candidate, and the candidate mass is constrained to the corresponding known value [10].

We define a photon candidate as an energy deposit in the ECL not associated with the extrapolated trajectory of any charged track. To suppress backgrounds from neutral hadrons, we require  $E(3 \times 3)/E(5 \times 5) \geq 0.6$ , where  $E(n \times n)$  denotes the energy deposited in an  $n \times n$  array of crystals centered on the highest-energy crystal (for Belle II, the four corner crystals of the  $5 \times 5$  array are excluded). The photon energy is required to exceed 50 MeV in the laboratory frame. At Belle II, BDT classifiers are used to suppress energy deposits from secondary hadronic interactions unrelated to the relevant collision and overlapping beam-induced photons [35].

The combined signal efficiencies (background rejection rates) of the two BDTs are approximately 89% (47%) and 89% (44%) for the charged and neutral channels, respectively.

The invariant masses of the reconstructed  $\Lambda_c^+$ ,  $\Xi_c^-$ , and  $\Xi_c^0$  candidates are required to lie within  $\pm 15$ ,  $\pm 18$ , and  $\pm 18$  MeV/ $c^2$  of their known values [10], respectively, corresponding in each case to approximately  $2.5\sigma$ . Each  $\Lambda_c^+$  and  $\Xi_c^{\prime-0}$  candidate is fitted to a common vertex, and the candidate mass is constrained to the corresponding known value [10]. The  $\Sigma_c(2455)^{++0}$  baryons are reconstructed via their decays into  $\Lambda_c^+\pi^\pm$ , with the signal region defined as  $2.446 < M(\Lambda_c^+\pi^\pm) < 2.464$  GeV/ $c^2$ . After applying this requirement, more than 95% of the signal events are retained. The sideband regions of  $M(\Lambda_c^+\pi^\pm)$  are defined as  $2.436 < M(\Lambda_c^+\pi^\pm) < 2.444$  GeV/ $c^2$  and  $2.466 < M(\Lambda_c^+\pi^\pm) < 2.494$  GeV/ $c^2$ . The  $\Xi_c^{\prime-0}$  baryons are reconstructed via their decays into  $\gamma\Xi_c^{\prime-0}$ , with the reconstructed masses required to be within  $\pm 20$  MeV/ $c^2$  of the known  $\Xi_c^{\prime-0}$  masses [10], corresponding in each case to approximately  $2.5\sigma$ . Vertex fits are applied to the  $\Sigma_c(2455)^{++0}$  and  $\Xi_c^{\prime-0}$  candidates, with their masses constrained to the known values [10].

The  $B^+$  and  $B^0$  candidates are reconstructed from the  $\Sigma_c(2455)^{++}\Xi_c^{\prime-}$  and  $\Sigma_c(2455)^0\Xi_c^0$  combinations, respectively. This implies four distinct reconstruction modes for each signal channel. A vertex fit is applied to the  $B$  candidates with a requirement of  $\chi^2/\text{ndf} < 20$ , where ndf is the number of degrees of freedom. The beam-constrained mass  $M_{bc}$  and the energy difference  $\Delta E$  are defined for  $B$  candidates as  $M_{bc} = \sqrt{E_{\text{beam}}^2 - (\sum_i \vec{p}_i)^2}$  and  $\Delta E = \sum_i E_i - E_{\text{beam}}$ , where  $E_{\text{beam}} = \sqrt{s}/2$  is the beam energy and  $(E_i, \vec{p}_i)$  is the four-momentum of the  $i$ th daughter of the  $B$  meson, all calculated in the  $e^+e^-$  c.m. system. Candidates satisfying  $M_{bc} > 5.27$  GeV/ $c^2$  (approximately  $2.5\sigma$ ) and  $|\Delta E| < 0.06$  GeV (approximately  $12\sigma$ ) are retained for further analysis. The distributions of  $M(\Lambda_c^+\pi^\pm)$  and  $M(\gamma\Xi_c^{\prime-0})$  for the reconstructed  $B^+ \rightarrow \Sigma_c(2455)^{++}\Xi_c^{\prime-}$  and  $B^0 \rightarrow \Sigma_c(2455)^0\Xi_c^0$  candidates in the combined Belle and Belle II data are shown in the appendix. Because the photon from the  $\Xi_c^{\prime-}$  decay has very low energy, many random low-energy photon candidates, such as residual neutral clusters in the electromagnetic calorimeter or photons from other particles in the event, can form incorrect combinations with the  $\Xi_c^{\prime-}$  candidates. This results in a large number of events with multiple candidates. After applying all the selection criteria, the fractions of events in signal simulation with multiple candidates are 60.5%–63.8% (54.3%–58.9%) for the charged channel and 61.0%–64.0% (53.8%–58.4%) for the neutral channel in Belle (Belle II), depending on the reconstruction mode. The corresponding average candidate multiplicities are 2.12–2.33 (1.93–2.13) for the charged channel and 2.15–2.29 (1.93–2.03) for the neutral channel in Belle (Belle II). For events with multiple

candidates, a best-candidate selection (BCS) is applied, retaining the candidate with the smallest  $\chi^2$  from the vertex and mass-constrained fits to the charmed baryons and the  $B$  meson. It was checked that the BCS procedure does not introduce peaking structures in the  $\Delta E$  distribution or distort its shape, and yields signal efficiencies of 73.0%–76.2% (72.5%–75.1%) for the charged channel and 73.5%–74.0% (72.0%–75.0%) for the neutral channel in Belle (Belle II).

It is estimated from simulation that after the BCS around 50% of the selected signal candidates are incorrectly reconstructed, and these are referred to as self-cross-feed (SCF) events. The SCF component exhibits a broad  $\Delta E$  distribution that is clearly distinguishable from the correctly reconstructed signal but overlaps significantly with the combinatorial background. The SCF events are not treated as signal when determining the branching fractions. To have better control of SCF, we define the sideband regions of  $M(\gamma\Xi_c^{\prime-0})$  as  $2508 < M(\gamma\Xi_c^{\prime-0}) < 2548$  MeV/ $c^2$  and  $2608 < M(\gamma\Xi_c^{\prime-0}) < 2658$  MeV/ $c^2$ . The centers of the sideband regions are about  $5\sigma$  away from the center of the signal region. The sideband regions contain a significant SCF contribution, with a shape in the  $\Delta E$  distribution similar to that observed in the signal region. To better constrain the SCF component in the signal extraction, we perform a simultaneous fit to the  $\Delta E$  distributions in the signal and sideband regions of  $M(\gamma\Xi_c^{\prime-0})$ . Backgrounds are studied using inclusive simulated samples [23] and data from the sidebands of  $M(\Lambda_c^+)$ ,  $M(\Lambda_c^+\pi^\pm)$ ,  $M(\Xi_c^{\prime-0})$ , and  $M_{bc}$  distributions. No peaking background is observed in the  $\Delta E$  distributions of events from these sidebands.

To extract the signal yield of  $B^+ \rightarrow \Sigma_c(2455)^{++}\Xi_c^{\prime-}$  or  $B^0 \rightarrow \Sigma_c(2455)^0\Xi_c^0$ , we perform simultaneous unbinned extended maximum-likelihood fits to the  $\Delta E$  distributions of four samples: events from the signal and sideband regions of  $M(\gamma\Xi_c^{\prime-0})$  in both Belle and Belle II data. The likelihood functions used to model the  $\Delta E$  distributions in the signal and sideband regions of  $M(\gamma\Xi_c^{\prime-0})$  are parametrized as

$$\mathcal{L} = \frac{e^{-(N_{\text{sig}}+N_{\text{scf}}+N_{\text{bkg}})}}{N!} \prod_i^N [N_{\text{sig}}\mathcal{F}_{\text{sig}} + N_{\text{scf}}\mathcal{F}_{\text{scf}} + N_{\text{bkg}}\mathcal{F}_{\text{bkg}}]$$

and

$$\mathcal{L}^{\text{sb}} = \frac{e^{-(N_{\text{sig}}^{\text{sb}}+N_{\text{scf}}^{\text{sb}}+N_{\text{bkg}}^{\text{sb}})}}{N^{\text{sb}}!} \prod_i^{N^{\text{sb}}} [N_{\text{sig}}^{\text{sb}}\mathcal{F}_{\text{sig}} + N_{\text{scf}}^{\text{sb}}\mathcal{F}_{\text{scf}}^{\text{sb}} + N_{\text{bkg}}^{\text{sb}}\mathcal{F}_{\text{bkg}}^{\text{sb}}],$$

respectively. Here,  $\mathcal{F}^{(\text{sb})}$  is the probability density function (PDF), and  $N^{(\text{sb})}$  denotes the number of observed events. The signal PDF,  $\mathcal{F}_{\text{sig}}$ , is parameterized

by a double-Gaussian function with the same mean values. The fraction and parameters of the tail Gaussian, which represents the broader part of the distribution, are fixed to the values obtained from simulation. The SCF PDFs,  $\mathcal{F}_{\text{scf}}^{(\text{sb})}$ , are modeled using the nonparametric kernel density estimation [36] derived from simulation. The combinatorial background PDFs,  $\mathcal{F}_{\text{bkg}}^{(\text{sb})}$ , are described by first-order polynomials with free parameters. The quantities  $N_{\text{sig}}^{(\text{sb})}$ ,  $N_{\text{scf}}^{(\text{sb})}$ , and  $N_{\text{bkg}}^{(\text{sb})}$  represent the signal, SCF, and combinatorial background yields, respectively. The signal (SCF) yields satisfy  $N_{\text{sig}(\text{scf})}^{\text{sb}} = f_{\text{sig}(\text{scf})} N_{\text{sig}(\text{scf})}$ , where  $f_{\text{sig}(\text{scf})}$  is defined as the ratio of the signal (SCF) yield in the sideband regions to that in the signal region of  $M(\gamma\bar{\Xi}_c^{-,0})$ , as estimated from simulation. The values of  $f_{\text{sig}}$  and  $f_{\text{scf}}$  are fixed by simulation to 0.02 (0.05) and 1.9 (1.8) for the charged channel and 0.01 (0.04) and 1.8 (1.6) for the neutral channel in Belle (Belle II), respectively. The event yields are determined from the fit, with the signal yields in the Belle and Belle II datasets constrained to follow the expected ratio for a common branching fraction.

Figure 2 shows the  $\Delta E$  distributions of candidates reconstructed in the signal and sideband regions of  $M(\gamma\bar{\Xi}_c^{-,0})$  in the combined Belle and Belle II data, with fit results overlaid. The fitted signal yields for the decays  $B^+ \rightarrow \Sigma_c(2455)^{++}\bar{\Xi}_c^{\prime-}$  and  $B^0 \rightarrow \Sigma_c(2455)^0\bar{\Xi}_c^{\prime0}$  are  $62.3 \pm 11.3$  and  $30.7 \pm 7.6$ , respectively, with statistical significances of  $8.6\sigma$  and  $6.9\sigma$ . The statistical significances are calculated using  $-2\ln(\mathcal{L}_0/\mathcal{L}_{\text{max}})$ , accounting for the difference in the number of degrees of freedom ( $\Delta\text{ndf}=3$ ), where  $\mathcal{L}_0$  and  $\mathcal{L}_{\text{max}}$  are the likelihood values obtained from fits without and with the signal and SCF components, respectively.

To evaluate the signal significances including systematic uncertainties, we repeat the significance calculation using the same alternative fits as those used to evaluate the systematic uncertainties associated with the fit models, with the relevant variations considered in combination. The most conservative values, corresponding to the smallest significances obtained among all tested cases, are  $6.4\sigma$  for the  $B^+ \rightarrow \Sigma_c(2455)^{++}\bar{\Xi}_c^{\prime-}$  channel and  $5.3\sigma$  for the  $B^0 \rightarrow \Sigma_c(2455)^0\bar{\Xi}_c^{\prime0}$  channel. These values are taken as the final signal significances after incorporating systematic effects.

The branching fractions of  $B^+ \rightarrow \Sigma_c(2455)^{++}\bar{\Xi}_c^{\prime-}$  and  $B^0 \rightarrow \Sigma_c(2455)^0\bar{\Xi}_c^{\prime0}$  decays are calculated using

$$\mathcal{B} = \frac{N_{\text{sig}}}{2f_{+-/00}[N_{\Upsilon(4S)}^{\text{B}} \sum_i (\varepsilon_i^{\text{B}} \mathcal{B}_i) + N_{\Upsilon(4S)}^{\text{B2}} \sum_i (\varepsilon_i^{\text{B2}} \mathcal{B}_i)]}.$$

Here,  $N_{\text{sig}}$  represents the number of fitted  $B^+ \rightarrow \Sigma_c(2455)^{++}\bar{\Xi}_c^{\prime-}$  or  $B^0 \rightarrow \Sigma_c(2455)^0\bar{\Xi}_c^{\prime0}$  signal events in the combined Belle and Belle II datasets;  $N_{\Upsilon(4S)}^{\text{B,B2}}$  denotes the total number of  $\Upsilon(4S)$  events in the Belle or Belle II datasets;  $f_{+-/00}$  refers to the fraction of charged

( $f_{+-} = 0.5113_{-0.0108}^{+0.0073}$ ) or neutral ( $f_{00} = 0.4861_{-0.0080}^{+0.0074}$ )  $B\bar{B}$  pairs [37]; the term  $\sum_i (\varepsilon_i^{\text{B,B2}} \mathcal{B}_i)$  represents the sum of the reconstruction efficiencies  $\varepsilon_i^{\text{B,B2}}$  (for Belle or Belle II) times the corresponding secondary branching fractions  $\mathcal{B}_i$  over all the reconstructed modes. The values of the aforementioned quantities, as obtained from the fit, and the calculated branching fractions are summarized in Table I.

The following sources of systematic uncertainties are the most important ones, and have been considered in this work: the detection-efficiency (DE) uncertainties ( $\sigma_{\text{DE}}$ ), the statistical uncertainty on the efficiency determined from simulation ( $\sigma_{\text{eff}}$ ), the uncertainties of the branching fractions of intermediate states ( $\sigma_{\mathcal{B}_i}$ ), the uncertainty of the total number of  $\Upsilon(4S)$  events ( $\sigma_{N_{\Upsilon(4S)}}$ ), the uncertainty on the fraction of charged or neutral  $B\bar{B}$  events ( $\sigma_{f_{+-/00}}$ ), the uncertainty associated with the BCS strategy ( $\sigma_{\text{BCS}}$ ), and uncertainties related to the fit models ( $\sigma_{\text{fit}}$ ). We explain the sources of systematics in the following, and summarize their values in Table II, where the total uncertainty ( $\sigma_{\text{total}}$ ) is calculated by adding the individual contributions in quadrature.

The DE uncertainties include contributions from tracking efficiency, PID efficiency, and the reconstruction of photon,  $K_S^0$ , and  $\bar{\Lambda}$  candidates, which are estimated using data control samples. The tracking efficiency uncertainty depends on the particle charge, momentum, and polar angle, and ranges from 0.32% to 1.22% (0.38% to 1.43%) per track in Belle (Belle II). These uncertainties are determined from control samples of  $D^{*+} \rightarrow D^0(\rightarrow K_S^0\pi^+\pi^-)\pi^+$  for Belle, and  $\bar{B}^0 \rightarrow D^{*+}(\rightarrow D^0\pi^+)\pi^-$  and  $e^+e^- \rightarrow \tau^+\tau^-$  for Belle II. The slightly larger tracking uncertainties in Belle II result from the limited statistics of the control samples. The PID efficiency uncertainties are estimated to be 1.0% (0.8%) for pions, 1.3% (1.1%) for kaons, and 2.2% (0.7%) for protons in Belle (Belle II) [30, 31]. The photon reconstruction uncertainty is 2.0% (1.6%) in Belle (Belle II), as determined from control samples of radiative Bhabha (radiative muon-pair) events. The  $K_S^0$  reconstruction uncertainty is 1.6% and 2.1% in Belle and Belle II, respectively, evaluated using control samples of  $D^{*+} \rightarrow D^0(\rightarrow K_S^0\pi^0)\pi^+$  and  $D^{*+} \rightarrow D^0(\rightarrow K_S^0\pi^+\pi^-)\pi^+$ . The  $\bar{\Lambda}$  reconstruction uncertainty is 2.2% and 1.3% in Belle and Belle II, respectively, evaluated using control samples of  $\bar{\Lambda} \rightarrow \bar{p}\pi^+$  and  $\bar{\Lambda}_c^- \rightarrow \bar{\Lambda}(\rightarrow \bar{p}\pi^+)\pi^-$ . The individual uncertainties for the different reconstruction modes in Belle and Belle II are weighted by  $N_{\Upsilon(4S)}^{\text{B,B2}} \times (\varepsilon_i^{\text{B,B2}} \mathcal{B}_i)$  and then combined. Assuming these uncertainties are independent and adding them in quadrature, the DE uncertainties are evaluated to be 2.7% and 2.4% for the charged and neutral channels, respectively.

The statistical uncertainty on the simulation-based efficiency is at most 1.0%. The relative uncertainties

$$\int \mathcal{L} dt = 711 \text{ fb}^{-1} (\text{Belle}) + 492 \text{ fb}^{-1} (\text{Belle II})$$

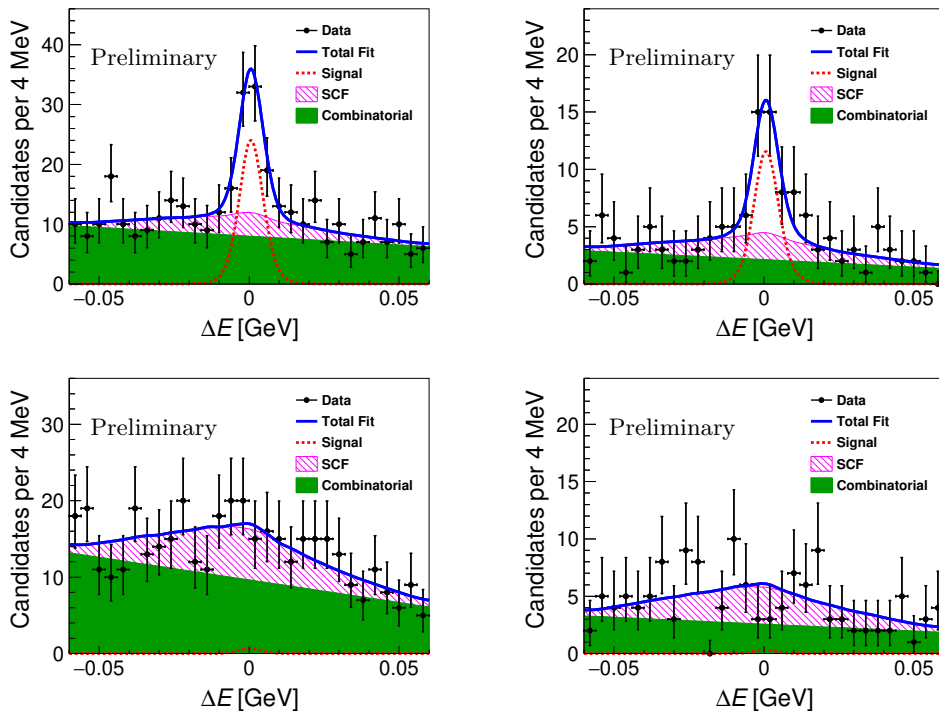


FIG. 2: Distributions of  $\Delta E$  for the reconstructed (left)  $B^+ \rightarrow \Sigma_c(2455)^{++}\bar{\Xi}_c^{\prime-}$  and (right)  $B^0 \rightarrow \Sigma_c(2455)^0\bar{\Xi}_c^{\prime0}$  candidates in the (top) signal and (bottom) sideband regions of  $M(\gamma\bar{\Xi}_c^{\prime-0})$  in the combined Belle and Belle II data. Points with error bars denote the data. The blue solid and red dashed curves represent the total fit results and fitted signal components, respectively, while the magenta hatched and green filled histograms represent the fitted SCF and combinatorial background components.

TABLE I: Summary of the fitted signal yields, the values of  $\sum_i(\epsilon_i^{\text{B},\text{B}2}\mathcal{B}_i)$ , and the measured branching fractions of  $B^+ \rightarrow \Sigma_c(2455)^{++}\bar{\Xi}_c^{\prime-}$  and  $B^0 \rightarrow \Sigma_c(2455)^0\bar{\Xi}_c^{\prime0}$  decays. We list only the statistical uncertainties of the signal yields. For the branching fractions, the first and second uncertainties are statistical and systematic, respectively, while the third originates from the absolute branching fractions of the  $\bar{\Xi}_c^{\prime-0}$  decays [10].

	$N_{\text{sig}}$	$\sum_i(\epsilon_i^{\text{B}}\mathcal{B}_i) (10^{-5})$	$\sum_i(\epsilon_i^{\text{B}2}\mathcal{B}_i) (10^{-5})$	$\mathcal{B} (10^{-3})$
$B^+$	$62.3 \pm 11.3$	2.44	3.33	$1.68 \pm 0.31 \pm 0.12_{-0.54}^{+1.49}$
$B^0$	$30.7 \pm 7.6$	1.52	2.47	$1.28 \pm 0.32 \pm 0.10_{-0.21}^{+0.30}$

of the absolute branching fractions of  $\Lambda_c^+ \rightarrow pK^-\pi^+$ ,  $\Lambda_c^+ \rightarrow pK_S^0$ ,  $K_S^0 \rightarrow \pi^+\pi^-$ ,  $\bar{\Xi}_c^- \rightarrow \bar{\Xi}^+\pi^-\pi^-$ ,  $\bar{\Xi}_c^- \rightarrow \bar{p}K^+\pi^-$ ,  $\bar{\Xi}_c^0 \rightarrow \bar{\Xi}^+\pi^-$ ,  $\bar{\Xi}_c^0 \rightarrow \bar{\Lambda}K^+\pi^-$ ,  $\bar{\Xi}^+ \rightarrow \Lambda\pi^+$ , and  $\bar{\Lambda} \rightarrow \bar{p}\pi^+$  are taken from Ref. [10]. Given the large uncertainties in the branching fractions of the intermediate decays  $\bar{\Xi}_c^- \rightarrow \bar{\Xi}^+\pi^-\pi^-$  (44.8%),  $\bar{\Xi}_c^- \rightarrow \bar{p}K^+\pi^-$  (48.4%),  $\bar{\Xi}_c^0 \rightarrow \bar{\Xi}^+\pi^-$  (18.9%), and  $\bar{\Xi}_c^0 \rightarrow \bar{\Lambda}K^+\pi^-$  (19.3%), which may be reduced by future measurements, we treat them separately as a third source of uncertainty. The branching fraction of each intermediate state except for the  $\bar{\Xi}_c^{\prime-0}$  is varied independently by  $\pm 1\sigma$ , with the resulting deviation from the nominal value taken as the corresponding systematic uncertainty. For the two decay modes of  $\bar{\Xi}_c^{\prime-0}$ , the branching fraction uncertainties are treated as fully correlated and are therefore varied simultaneously

by  $\pm 1\sigma$ . The uncertainties on the absolute branching fractions of  $\bar{\Xi}_c^-$ ,  $\bar{\Xi}_c^0$ , and other intermediate states are  $+88.3\%$ ,  $+23.6\%$ ,  $-31.9\%$ ,  $-16.1\%$ , and  $3.5\%$ , respectively. The uncertainties of  $N_{\Upsilon(4S)}^{\text{B},\text{B}2}$  are 1.4% for Belle and 1.5% for Belle II, and are combined into a total uncertainty weighted by  $N_{\Upsilon(4S)}^{\text{B},\text{B}2} \times \sum_i(\epsilon_i^{\text{B},\text{B}2}\mathcal{B}_i)$ . The uncertainties of  $f_{+-}$  and  $f_{00}$  are 2.1% and 1.7%, respectively. To evaluate the uncertainty associated with the BCS strategy, we adopt an alternative BCS procedure in which the candidate with the minimum  $|M(\gamma\bar{\Xi}_c^{\prime-0}) - m(\bar{\Xi}_c^{\prime-0})|$  is retained instead of the nominal criterion, where  $m(\bar{\Xi}_c^{\prime-0})$  denotes the known mass of the  $\bar{\Xi}_c^{\prime-0}$  baryon [10]. The resulting change in the measured branching fraction is taken as the corresponding systematic uncertainty. This uncertainty is estimated to be 2.5% and 3.6% for the charged and

neutral channels, respectively.

The systematic uncertainties associated with the fit models arise from the signal PDF, the background PDFs, the choice of  $M(\gamma\Xi_c^{-,0})$  sideband regions, the modeling of the SCF components, the parameters  $f_{\text{sig}}$  and  $f_{\text{scf}}$ , and the possible peaking background from non-resonant  $\Lambda_c^+\pi^\pm$  combinations in the  $\Sigma_c(2455)^{+,0}$  signal region. The signal PDF is replaced by a triple-Gaussian function, and the resulting systematic uncertainty is negligible. To evaluate the systematic uncertainty associated with the background PDFs, pseudo-experiments are generated using a second-order polynomial or an exponential function, with parameters taken from the corresponding alternative fits to data, while keeping the signal component unchanged. Each pseudo-experiment is fitted with the nominal background model, and the largest difference between the mean fitted signal yield and the corresponding input yield is taken as systematic uncertainty. To assess the uncertainty associated with the choice of  $M(\gamma\Xi_c^{-,0})$  sideband regions, the lower and upper sideband regions are shifted simultaneously toward lower and higher mass, respectively, by 1, 2, 3, 4, and 5 MeV, with their widths kept unchanged. For the largest variation, the mass range between the lowest and highest sideband boundaries corresponds to about  $15\sigma$  of the  $M(\gamma\Xi_c^{-,0})$  resolution. The largest deviation of the fitted signal yield from the nominal result is assigned as the systematic uncertainty. The SCF-related uncertainty is evaluated by interchanging the SCF PDFs derived from the  $M(\gamma\Xi_c^{-,0})$  signal and sideband regions, with the resulting change in the fitted signal yield taken as the systematic uncertainty. To estimate the systematic uncertainty associated with  $f_{\text{sig}}$ , we treat  $f_{\text{sig}}$  as a free parameter and repeat the fit. The deviation from the nominal result is taken as the systematic uncertainty. The uncertainty related to  $f_{\text{scf}}$  is covered by the variations of the sideband regions and the interchange of the SCF PDFs, which probe the uncertainty in the SCF modeling. The possible peaking background from non-resonant  $\Lambda_c^+\pi^\pm$  combinations to the  $\Delta E$  distribution is studied using events in the  $M(\Lambda_c^+\pi^\pm)$  sideband regions, and a simultaneous fit to the  $\Delta E$  distributions in the  $M(\gamma\Xi_c^{-,0})$  signal region, the  $M(\gamma\Xi_c^{-,0})$  sideband regions, and the  $M(\Lambda_c^+\pi^\pm)$  sideband regions for Belle and Belle II datasets is performed. The resulting change in the fitted signal yield is smaller than 0.5% for both the charged and neutral channels, and is therefore neglected. The systematic uncertainties associated with the background PDFs, the choice of  $M(\gamma\Xi_c^{-,0})$  sideband regions, the SCF components, and the value of  $f_{\text{sig}}$  are estimated to be 2.6% (3.1%), 2.4% (1.6%), 1.5% (2.8%), and 2.0% (2.0%) for charged channel (neutral), respectively. All of these contributions are summed in quadrature to obtain the total systematic uncertainty related to the fit models.

In summary, we report the first observation of the decays  $B^+ \rightarrow \Sigma_c(2455)^{++}\Xi_c^-$  and  $B^0 \rightarrow \Sigma_c(2455)^0\Xi_c^0$ , using data samples corresponding to  $771.6 \times 10^6$  and

TABLE II: Summary of fractional systematic uncertainties (%) on the  $\mathcal{B}(B^+ \rightarrow \Sigma_c(2455)^{++}\Xi_c^-)$  and  $\mathcal{B}(B^0 \rightarrow \Sigma_c(2455)^0\Xi_c^0)$ . The sources of all uncertainties are described in the text.

	$\sigma_{\text{DE}}$	$\sigma_{\text{eff}}$	$\sigma_{\mathcal{B}_i}$	$\sigma_{N_{\Upsilon(4S)}}$	$\sigma_{f_{+-/00}}$	$\sigma_{\text{BCS}}$	$\sigma_{\text{fit}}$	$\sigma_{\text{total}}$
$B^+$	2.7	1.0	3.5	1.0	2.1	2.5	4.3	7.2
$B^0$	2.4	1.0	3.5	1.0	1.7	3.6	4.9	7.8

$520.6 \times 10^6$   $\Upsilon(4S)$  events collected by the Belle and Belle II experiments, respectively. This represents the first observation of  $B$ -meson decays into a pair of charmed baryon-antibaryon states that belong to the same  $SU(3)$  flavor sextet. The branching fractions are measured to be  $\mathcal{B}(B^+ \rightarrow \Sigma_c(2455)^{++}\Xi_c^-) = (1.68 \pm 0.31 \pm 0.12_{-0.54}^{+1.49}) \times 10^{-3}$  and  $\mathcal{B}(B^0 \rightarrow \Sigma_c(2455)^0\Xi_c^0) = (1.28 \pm 0.32 \pm 0.10_{-0.21}^{+0.30}) \times 10^{-3}$ , where the uncertainties are statistical, systematic, and from the absolute branching fractions of  $\Xi_c^-$  and  $\Xi_c^0$  decays, respectively. The measured branching fractions are two to three times larger than those of  $B^+ \rightarrow \Sigma_c(2455)^{++}\Xi_c^-$  and  $B^0 \rightarrow \Sigma_c(2455)^0\Xi_c^0$  [11], despite the smaller available phase space for these decays. This observation may indicate nontrivial dynamical effects in baryonic  $B$  decays that enhance or suppress specific decay modes.

This work, based on data collected using the Belle II detector, which was built and commissioned prior to March 2019, was supported by Higher Education and Science Committee of the Republic of Armenia Grant No. 23LCG-1C011; Australian Research Council and Research Grants No. DP200101792, No. DP210101900, No. DP210102831, No. DE220100462, No. LE210100098, and No. LE230100085; Austrian Federal Ministry of Education, Science and Research, Austrian Science Fund (FWF) Grants DOI: 10.55776/P34529, DOI: 10.55776/J4731, DOI: 10.55776/J4625, DOI: 10.55776/M3153, and DOI: 10.55776/PAT1836324, and Horizon 2020 ERC Starting Grant No. 947006 ‘‘InterLeptons’’; Natural Sciences and Engineering Research Council of Canada, Digital Research Alliance of Canada, and Canada Foundation for Innovation; National Key R&D Program of China under Contract No. 2024YFA1610503, and No. 2024YFA1610504 National Natural Science Foundation of China and Research Grants No. 11575017, No. 11761141009, No. 11705209, No. 11975076, No. 12135005, No. 12150004, No. 12161141008, No. 12405099, No. 12475093, and No. 12175041, China Postdoctoral Science Foundation (CPSF) under Grant No. 2024M760485, and China Postdoctoral Fellowship Program of CPSF under Grant No. GZC20240303, and Shandong Provincial Natural Science Foundation Project ZR2022JQ02; the Czech Science Foundation Grant No. 22-18469S, Regional funds of EU/MEYS: OPJAK FORTE CZ.02.01.01/00/22\_008/0004632 and Charles University Grant Agency project No. 246122;

European Research Council, Seventh Framework PIEF-GA-2013-622527, Horizon 2020 ERC-Advanced Grants No. 267104 and No. 884719, Horizon 2020 ERC-Consolidator Grant No. 819127, Horizon 2020 Marie Skłodowska-Curie Grant Agreement No. 700525 “NIOBE” and No. 101026516, and Horizon Europe Marie Skłodowska-Curie Staff Exchange project JENNIFER3 Grant Agreement No. 101183137 (European grants); L’Institut National de Physique Nucléaire et de Physique des Particules (IN2P3) du CNRS under Project Identification No. CNRS-IN2P3-14-PP-033 and L’Agence Nationale de la Recherche (ANR) under Grant No. ANR-23-CE31- 0018 and ANR-25-CE31-1333 (France); BMFTR, DFG, HGF, MPG, and AvH Foundation (Germany); Department of Atomic Energy under Project Identification No. RTI 4002, Department of Science and Technology, and UPES SEED funding programs No. UPES/R&D-SEED-INFRA/17052023/01 and No. UPES/R&D-SOE/20062022/06 (India); Israel Science Foundation Grant No. 2476/17, U.S.-Israel Binational Science Foundation Grant No. 2016113, and Israel Ministry of Science Grant No. 3-16543; Istituto Nazionale di Fisica Nucleare and the Research Grants BELLE2, and the ICSC – Centro Nazionale di Ricerca in High Performance Computing, Big Data and Quantum Computing, funded by European Union – NextGenerationEU; Japan Society for the Promotion of Science, Grant-in-Aid for Scientific Research Grants No. 16H03993, No. 16H06492, No. 16K05323, No. 17H01133, No. 17H05405, No. 18K03621, No. 18H03710, No. 18H05226, No. 19H00682, No. 20H05850, No. 20H05858, No. 22H00144, No. 22K14056, No. 22K21347, No. 23H05433, No. 26220706, No. 26400255, and No. 26H02056, and the Ministry of Education, Culture, Sports, Science, and Technology (MEXT) of Japan; National Research Foundation (NRF) of Korea Grants No. 2021R1-F1A-1064008, No. 2022R1-A2C-1003993, No. RS-2018-NR031074, No. RS-2021-NR060129, No. RS-2024-00354342, No. RS-2025-02219521, No. RS-2026-25471491, No. RS-2026-25480677, and No. RS-2026-25486791, Radiation Science Research Institute, Foreign Large-Size Research Facility Application Supporting project, the Global Science Experimental Data Hub Center, the Korea Institute of Science and Technology Information (K26L1M2C3) and KREONET/GLORIAD; Universiti Malaya RU grant, Akademi Sains Malaysia, and Ministry of Education Malaysia; Frontiers of Science Program Contracts No. FOINS-296, No. CB-221329, No. CB-236394, No. CB-254409, and No. CB-180023, and SEP-CINVESTAV Research Grant No. 237 (Mexico); the Polish Ministry of Science and Higher Education and the National Science Center; the Ministry of Science and Higher Education of the Russian Federation and the HSE University Basic Research Program, Moscow; University of Tabuk Research Grants No. S-0256-1438 and No. S-0280-1439 (Saudi Arabia); Slovenian Research Agency

and Research Grants No. J1-50010 and No. P1-0135; Ikerbasque, Basque Foundation for Science, State Agency for Research of the Spanish Ministry of Science and Innovation through Grant No. PID2022-136510NB-C33, Spain, Agencia Estatal de Investigacion, Spain Grant No. RYC2020-029875-I and Generalitat Valenciana, Spain Grant No. CIDEGENT/2018/020; The Knut and Alice Wallenberg Foundation (Sweden), Contracts No. 2021.0174, No. 2021.0299, and No. 2023.0315; National Science and Technology Council, and Ministry of Education (Taiwan); Thailand Center of Excellence in Physics; TUBITAK ULAKBIM (Turkey); National Research Foundation of Ukraine, Project No. 2020.02/0257, and Ministry of Education and Science of Ukraine; the U.S. National Science Foundation and Research Grants No. PHY-1913789 and No. PHY-2111604, and the U.S. Department of Energy and Research Awards No. DE-AC06-76RLO1830, No. DE-SC0007983, No. DE-SC0009824, No. DE-SC0009973, No. DE-SC0010007, No. DE-SC0010073, No. DE-SC0010118, No. DE-SC0010504, No. DE-SC0011784, No. DE-SC0012704, No. DE-SC0019230, No. DE-SC0021616, No. DE-SC0022350, No. DE-SC0023470; and the Vietnam Academy of Science and Technology (VAST) under Grant No. DL0000.05/26-27.

These acknowledgements are not to be interpreted as an endorsement of any statement made by any of our institutes, funding agencies, governments, or their representatives.

We thank the SuperKEKB team for delivering high-luminosity collisions; the KEK cryogenics group for the efficient operation of the detector solenoid magnet and IBelle on site; the KEK Computer Research Center for on-site computing support; the NII for SINET6 network support; and the raw-data centers hosted by BNL, DESY, GridKa, IN2P3, INFN, and the University of Victoria.

### Data Availability

The full Belle II data are not publicly available. The collaboration will consider requests for access to the data that support this article.

### Appendix: Distributions of $M(\Lambda_c^+ \pi^\pm)$ and $M(\gamma \Xi_c^{\prime-0})$

Figure 3 shows the distributions of  $M(\Lambda_c^+ \pi^\pm)$  and  $M(\gamma \Xi_c^{\prime-0})$  for the reconstructed  $B^+ \rightarrow \Sigma_c(2455)^{++} \Xi_c^{\prime-}$  and  $B^0 \rightarrow \Sigma_c(2455)^{0} \Xi_c^{\prime-0}$  candidates in the combined Belle and Belle II data before the application of the BCS. Clear  $\Sigma_c(2455)^{++0}$  and  $\Xi_c^{\prime-0}$  signals are seen in data. The magenta arrows indicate the defined

signal regions for the  $\Sigma_c(2455)^{++0}$  and  $\Xi_c^{\prime-0}$  candidates, while the green arrows indicate the corresponding

sideband regions, with a total width twice that of the corresponding signal region.

- 
- [1] H. Y. Cheng, Nucl. Phys. B, Proc. Suppl. **163**, 68 (2007).  
 [2] R. Chistov, J. Phys. Conf. Ser. **675**, 022007 (2016).  
 [3] Ed. A. J. Bevan, B. Golob, Th. Mannel, S. Prell, and B. D. Yabsley, Eur. Phys. J. C **74**, 3026 (2014).  
 [4] Y. K. Hsiao, S. Y. Tsai, C. C. Lih, and E. Rodrigues, J. High Energy Phys. **04**, 035 (2020).  
 [5] Y. K. Hsiao, J. High Energy Phys. **11**, 117 (2023).  
 [6] R. Chistov *et al.* (Belle Collaboration), Phys. Rev. D **74**, 111105 (2006).  
 [7] B. Aubert *et al.* (BaBar Collaboration), Phys. Rev. D **77**, 031101 (2008).  
 [8] Y. Li *et al.* (Belle Collaboration), Phys. Rev. D **100**, 112010 (2019).  
 [9] R. Aaij *et al.* (LHCb Collaboration), Phys. Rev. Lett. **136**, 061802 (2026).  
 [10] S. Navas *et al.* (Particle Data Group), Phys. Rev. D **110**, 030001 (2024) and 2025 update.  
 [11] M. Abumusabh *et al.* (Belle and Belle II Collaborations), Phys. Rev. D **112**, L051101 (2025).  
 [12] A. Abashian *et al.* (Belle Collaboration), Nucl. Instrum. Meth. A **479**, 117 (2002).  
 [13] T. Abe *et al.* (Belle II Collaboration), arXiv:1011.0352.  
 [14] J. Brodzicka *et al.* (Belle Collaboration), Prog. Theor. Exp. Phys. **2012**, 04D001 (2012).  
 [15] I. Adachi *et al.* (Belle Collaboration), Chin. Phys. C **49**, 013001 (2025).  
 [16] S. Kurokawa and E. Kikutani, Nucl. Instrum. Meth. A **499**, 1 (2003), and other papers included in this volume; T. Abe *et al.*, Prog. Theor. Exp. Phys. **2013**, 03A001 (2013), and references therein.  
 [17] K. Akai *et al.* (SuperKEKB Accelerator Team), Nucl. Instrum. Meth. A **907**, 188 (2018).  
 [18] D. J. Lange, Nucl. Instrum. Meth. A **462**, 152 (2001).  
 [19] T. Sjöstrand, S. Mrenna, and P. Z. Skands, J. High Energy Phys. **05**, 026 (2006).  
 [20] T. Sjöstrand *et al.*, Comput. Phys. Commun. **191**, 159 (2015).  
 [21] E. Barberio, B. van Eijk, and Z. Was, Comput. Phys. Commun. **66**, 115 (1991).  
 [22] Z. J. Liptak *et al.*, Nucl. Instrum. Meth. A **1040**, 167168. (2022).  
 [23] X. Y. Zhou, S. X. Du, G. Li, and C. P. Shen, Comput. Phys. Commun. **258**, 107540 (2021).  
 [24] S. Jadach, B. F. L. Ward, and Z. Was, Comput. Phys. Commun. **130**, 260 (2000).  
 [25] R. Brun *et al.*, GEANT3: user's guide Geant 3.10, Geant 3.11, CERN Report No. DD/EE/84-1, 1984.  
 [26] S. Agostinelli *et al.* (GEANT4 Collaboration), Nucl. Instrum. Meth. A **506**, 250 (2003).  
 [27] T. Kuhr, C. Pulvermacher, M. Ritter, T. Hauth, and N. Braun (Belle II Framework Software Group), Comput. Softw. Big Sci. **3**, 1 (2019).  
 [28] M. Gelb *et al.* Comput. Softw. Big Sci. **2**, 9 (2018).  
 [29] G. Punzi, eConf C030908, MODT002 (2003).  
 [30] E. Nakano, Nucl. Instrum. Meth. A **494**, 402 (2002).  
 [31] I. Adachi *et al.* (Belle II Collaboration), Eur. Phys. J. C **85**, 1237 (2025).  
 [32] H. Nakano *et al.* (Belle Collaboration) Phys. Rev. D **97**, 092003 (2018).  
 [33] F. Abudinén *et al.* (Belle and Belle II Collaborations), J. High Energy Phys. **02**, 063 (2022).  
 [34] J. Y. Lee *et al.* (Belle Collaboration) Phys. Rev. D **103**, 052005 (2021).  
 [35] P. Cheema, EPJ Web Conf. **295**, 09035 (2024).  
 [36] K. S. Cranmer, Comput. Phys. Commun. **136**, 198 (2001).  
 [37] S. Banerjee *et al.* (Heavy Flavor Averaging Group), Phys. Rev. D **113**, 012008 (2026), with specific result from doi:10.5281/zenodo.19210609.

$$\int \mathcal{L} dt = 711 \text{ fb}^{-1} (\text{Belle}) + 492 \text{ fb}^{-1} (\text{Belle II})$$

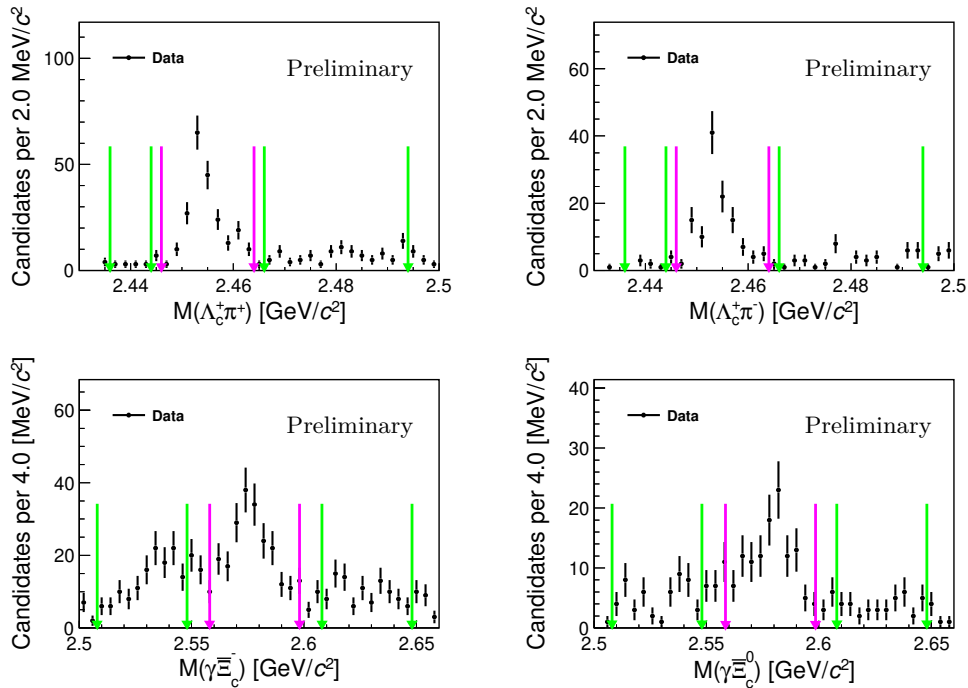


FIG. 3: Distributions of (top)  $M(\Lambda_c^+ \pi^\pm)$  and (bottom)  $M(\gamma \Xi_c^{\prime-0})$  for the reconstructed (left)  $B^+ \rightarrow \Sigma_c(2455)^{++} \Xi_c^{\prime-}$  and (right)  $B^0 \rightarrow \Sigma_c(2455)^0 \Xi_c^{\prime0}$  candidates in the combined Belle and Belle II data. Points with error bars represent the data. The magenta arrows indicate the defined signal regions for the  $\Sigma_c(2455)^{++0}$  and  $\Xi_c^{\prime-0}$  candidates, while the green arrows indicate the corresponding sideband regions.